JOURNAL OF AIRCRAFT
Vol. 46, No. 5, September–October 2009

Calculation of Rotorcraft Inflow Coefficients Using Blade Flapping Measurements

S. S. Houston* and D. G. Thomson†
University of Glasgow, Glasgow, Scotland G12 8QQ, United Kingdom

DOI: 10.2514/1.40540

Induced velocity gives rise to an important component of the angle of attack experienced by a blade element and, hence, the rotor loads. Finite-state induced-velocity models can be found in rotorcraft codes that require fast computation but cannot replicate real flowfield features. However, they do encapsulate in a simple and intuitive way the impact of real wakes on rotorcraft dynamics and hence are popular in codes that are used to study vehicle flight mechanics such as stability, control, and handling qualities. Explicit verification of these models is not possible, but implicit verification is possible if blade flapping is known; and this paper presents results from flight tests of a light gyroplane fitted with a two-bladed teetering rotor instrumented to measure the rotor flapping behavior. An appropriate model structure is developed to allow calculation of induced-velocity components from steady-flight flapping data recorded across the aircraft's level-flight speed range. Very good agreement is obtained between flight and theory in respect to the uniform and longitudinal components, correlating well with previous studies. However, the lateral component is very poorly correlated, and this is attributed to strong nontrapezoidal behavior in the real wake. Notwithstanding this, it is concluded that the simple finite-state, induced-velocity model is a valid tool for gyroplane flight mechanics studies and rotorcraft autorotation in general.

Nomenclature

a_0	=	blade section lift coefficient at the zero angle of attack
a_1	=	blade section lift-curve slope, rad^{-1}
C_T	=	thrust coefficient
c	=	blade chord, m
dM_{flap}	=	elemental blade flap moment about the hinge, Nm
dr	=	elemental length, m
I_β	=	blade flap moment of inertia about the hinge, kgm^2
L_{aero}	=	rotor aerodynamic rolling moment, Nm
M_{aero}	=	rotor aerodynamic pitching moment, Nm
R	=	rotor radius, m
r	=	radial location of a location on blade from the flap hinge, m
T_{aero}	=	rotor aerodynamic thrust, N
U_T	=	component of the blade element relative airflow tangential to the blade, ms^{-1}
U_p	=	component of the blade element relative airflow normal to blade, ms^{-1}
V	=	airspeed, ms^{-1}
v_T	=	total velocity at the rotor disc center, ms^{-1}
v_i	=	induced velocity, ms^{-1}
v_{i0m}	=	momentum induced velocity, ms^{-1}
v_m	=	mass flow parameter, ms^{-1}
v_0	=	uniform component of the induced velocity, ms^{-1}
v_{1c}	=	longitudinal component of induced velocity, ms^{-1}
v_{1s}	=	lateral component of induced velocity, ms^{-1}
w_{hub}	=	velocity normal to the rotor disc, ms^{-1}
α	=	blade element angle of attack, rad
β	=	blade flapping angle, rad
β_t	=	teeter angle, rad
β_0	=	rotor-coning angle, rad
β_{1c}	=	rotor disc longitudinal tilt, rad
β_{1s}	=	rotor disc lateral tilt, rad
γ	=	rotor Lock number
θ	=	blade pitch angle, rad
θ_{tw}	=	blade twist distribution, rad/m
ρ	=	air density, kg/m^3
σ	=	rotor solidity
ϕ	=	blade element inflow angle, rad
χ	=	wake skew angle, rad
ψ	=	blade azimuth angle, rad
ψ_m	=	flight-measurement blade azimuth angle, rad
Ω	=	rotor speed, rad/s

Received 28 August 2008; revision received 9 May 2009; accepted for publication 11 May 2009.

*Senior Lecturer, Department of Aerospace Engineering; s.houston@aero.gla.ac.uk.

†Senior Lecturer, Department of Aerospace Engineering; d.thomson@aero.gla.ac.uk.

Introduction

THE induced-velocity distribution across the rotor disc is an integral element of a rotorcraft mathematical model because it constitutes a significant component of blade element angle of attack and hence loading. Codes are available to calculate the environment around the entire aircraft, naturally embodying real flowfield features such as blade–blade and rotor–rotor aerodynamic interactions [1]. However, most engineering models applied to stability, control, and handling quality studies use finite-state representations that mimic or emulate real-wake effects, because their computational demands are so much less than full-flowfield models [2]. Momentum-disc and actuator-disc theories underpin many of these modeling approaches. Model fidelity is normally checked by comparison with flight-test data, but either of these induced-velocity modeling approaches requires verification by implicit, rather than explicit, means due to the intrinsic complexity of the inflow distribution. This implicit approach takes advantage of the intimate relationship between rotor blade flapping and the induced velocity [3], and the relative ease with which blade flapping data can be obtained. The objective of this paper, therefore, is to validate a finite-state induced-velocity model, a novel aspect in reference to operation in autorotation. Blade flapping data measured during gyroplane flight trials is coupled with an appropriate model structure, allowing induced-velocity components to be calculated across the level-flight speed range of the aircraft.

Background

Verification of any inflow model requires an implicit, rather than explicit, approach, as the instrumentation required to measure and record induced velocity does not exist. Central to any implicit approach is the availability of blade flapping data, as inflow and

flapping are intimately related. Model structures that relate airframe motion, flapping, and inflow can also be used to extract inflow time constants from flight-test data [4,5]; hence, a complete picture of induced-velocity static and dynamic behavior can be obtained. Previous studies of note include use of lateral flapping data to examine nonuniform inflow model structures, in which one conclusion was that at low tip-speed ratios, a more sophisticated wake geometry calculation is required [6]. The simple three-state inflow model structure may be inadequate for capturing real flowfield features, but it remains an appropriate model structure to mimic wake contribution to rotor loads and hence vehicle behavior.

Contemporary interest in the flight mechanics of light gyroplanes stems from work initiated by the U.K. Civil Aviation Authority in the early 1990s, itself in response to a recommendation from the Air Accidents Investigation Branch of the Department of Trade that arose from concern about the fatal accident rate in the United Kingdom [7]. The subsequent research program involved mathematical modeling and wind-tunnel and flight testing, and has been reported widely [8–11]. An engineering model of vehicle behavior was acknowledged to be an indispensible tool for understanding aircraft flight mechanics, and the studies used a generic individual-blade, blade element formulation that can be configured as any helicopter or gyroplane if configuration-specific data are known. Verification is an important exercise to build confidence in model fidelity, and considerable effort has been expended both for gyroplane and helicopter applications of the model [10,12]. Comparisons with flight have included trim, stability and control derivatives, and nonlinear response to control inputs [13].

The finite-state, dynamic-inflow model embodied in these simulations has not been the focus of specific verification in its own right as, in principle, it is applicable to flight in autorotation and has been validated extensively in development by others [14]. A recent review of the dynamic-inflow model has suggested only a minor revision to a mass flow term is required for correctness in autorotation, but simulation indicates that this is inconsequential in practical application of the dynamic-inflow model [15]. Nonetheless, verification using gyroplane flight-test data enhances confidence in the applicability of dynamic inflow for autorotation and is a focused contribution to a sparse literature.

Model Structure for Inflow Calculation

The induced-velocity distribution across the rotor disc is represented by

$$v_i(r,\psi) = v_0 + v_{1s}(r/R)\sin\psi + v_{1c}(r/R)\cos\psi \tag{1}$$

In steady flight, the uniform and harmonic components are obtained from the dynamic-inflow model of Peters and HaQuang [2], but using Chen's presentation [16] expressed in terms of wake skew angle; viz

$$\begin{bmatrix} v_0 \\ v_{1s} \\ v_{1c} \end{bmatrix} = \begin{bmatrix} \frac{1}{2\rho\pi R^2 v_T} & 0 & \frac{15\pi\tan\chi/2}{64\rho\pi R^3 v_m} \\ 0 & \frac{-4}{\rho\pi R^3 v_m(1+\cos\chi)} & 0 \\ \frac{15\pi\tan\chi/2}{64\rho\pi R^2 v_T} & 0 & \frac{-4\cos\chi}{\rho\pi R^3 v_m(1+\cos\chi)} \end{bmatrix} \begin{bmatrix} T_{\text{aero}} \\ L_{\text{aero}} \\ M_{\text{aero}} \end{bmatrix} \tag{2}$$

where

$$v_T = \sqrt{V^2 + (v_{i0m} - w_{\text{hub}})^2} \tag{3}$$

$$v_m = \frac{V^2 + (v_{i0m} - w_{\text{hub}})(2v_{i0m} - w_{\text{hub}})}{v_T} \tag{4}$$

$$\tan\chi = \frac{V}{v_{i0m} - w_{\text{hub}}} \tag{5}$$

Implicit in this description is the use of wind axes, but a simple transformation is used to obtain body axes quantities if necessary. Note also that Peters and Haquang [2] present the model in terms of α, where $\alpha = 90 - \chi$ and

$$\tan\alpha = \frac{|v_{i0m} - w_{\text{hub}}|}{V} \tag{6}$$

The moment about the flapping hinge of a blade element is given by

$$dM_{\text{flap}} = (1/2)\rho(U_T^2 + U_p^2)cr(a_0 + a_1\alpha)dr \tag{7}$$

where

$$U_T = \Omega r + V\sin\psi \tag{8}$$

$$U_p = v_i(r,\psi) - w_{\text{hub}} + r\dot{\beta} + V\beta\cos\psi \tag{9}$$

$$\alpha = \theta - \phi \tag{10}$$

Modeling blades as rigid and attached to the hub by means of hinges (and springs if appropriate) is a well-accepted process in rotorcraft simulation [17]. Johnson [18] describes the mathematical equivalence of such a rotor with an articulated rotor of zero-hinge offset in terms of tip-path plane tilt; in terms of the coning motion, the blades have cantilever root restraint. A separate study quantifies the specific nature of the restraint on this aircraft, further confirming that, in this case, the modeling approach is valid [19]. In summary then, the solution obtained for an articulated rotor with zero-hinge offset is also applicable to teetering rotors [18].

The typical, light, gyroplane, two-bladed, teetering rotor affects pitch and roll control by tilting the whole rotor hub; hence, no cyclic pitch is applied. However, some rotors do have a collective pitch control. In general then, the blade pitch is written

$$\theta = \theta_0 + r\theta_{tw} \tag{11}$$

and the inflow angle can be approximated by

$$\phi = U_p/U_T \tag{12}$$

Aircraft Instrumentation and Flight Test

The aircraft is shown in Fig. 1 and has been used to support U.K. Civil Aviation Authority-funded research into light gyroplane airworthiness. It is typical of this class of recreational aircraft in terms of rotor configuration and layout. It has a two-bladed, teetering main rotor without collective or cyclic pitch—pitch, and roll control is affected by tilting the entire rotor. The range of tilt is 18 deg longitudinally and laterally. The teeter or flapping range is 12 deg. The pusher propeller is driven through a reduction gearbox by a two-stroke gasoline engine. The experimental instrumentation fit comprises an inertial unit located behind the pilot that measures accelerations along all three body axes; angular velocities about these axes; and the roll, pitch, and heading angles. Flight control positions are measured using rotary potentiometers, and the air data system parameters are temperature, pressure, airspeed and the angles of attack and sideslip for which a probe fitted with vanes is attached to the nose of the aircraft. Rotor and propeller speeds are measured using Hall-effect sensors. A PC-based digital recording system is fitted with a selectable sample rate. Previous applications of the aircraft are given elsewhere [11] and have focussed principally on stability, control, and handling quality studies that included parameter estimation, model verification, and ADS-33 mission task element experiments.

Measurement of rotor teeter angle is by rotary potentiometer, two being fitted for redundancy. Rotor azimuth position is obtained by optical reader. Amplifiers are fitted to the rotor head and slip rings are used to transfer power and data between the fixed and rotating frames. The instrumentation assembly is shown in Fig. 2. This installation was designed for an airworthiness flight trial that did not include tests typical of a model verification exercise, such as multi-

Fig. 1 Montgomerie–Parsons gyroplane.

step or frequency sweep inputs for parameter estimation. However, a large number of trim test points were recorded, and these data are suitable for the analysis undertaken here. Figure 3 shows typical teeter and azimuth measurements. These are combined to give rotor disc lateral and longitudinal flapping angles as follows:

$$\beta_{1s} = -\beta_t \sin\psi_m \tag{13}$$

$$\beta_{1c} = -\beta_t \cos\psi_m \tag{14}$$

ψ_m is measured from the front of the rotor disc; β_t is positive for flap back in this position.

The three components of induced velocity v_0, v_{1s}, and v_{1c} can then be derived from these disc-tilt angles if Eqs. (8–12) are substituted into (7); integrated and harmonic balance performed to give

$$\beta_0 = \frac{\gamma}{2a_1\Omega^2R^2}\left\{\frac{(a_0 + a_1\theta_0)(\Omega^2R^2 + V^2)}{4} + Ra_1\theta_{tw}\left(\frac{\Omega^2R^2 + 5V^2/6}{5}\right) - \frac{\Omega R(v_0 - w_{\text{hub}})}{3} - \frac{Vv_{1s}}{6}\right\} \tag{15}$$

$$\beta_{1s}\left(\Omega R + \frac{V^2}{\Omega R}\right) = \frac{-4V\beta_0}{3} - v_{1c} \tag{16}$$

$$\beta_{1c} = \frac{-8V}{a_1(\Omega^2R^2 - V^2)}\left\{\frac{-\left(v_0 - w_{\text{hub}} + \Omega Rv_{1s}/2V\right)}{4} + \frac{\Omega R\left(\frac{a_0}{a_1} + \theta_0\right)}{3} + \frac{\Omega R^2\theta_{tw}}{4}\right\} \tag{17}$$

where

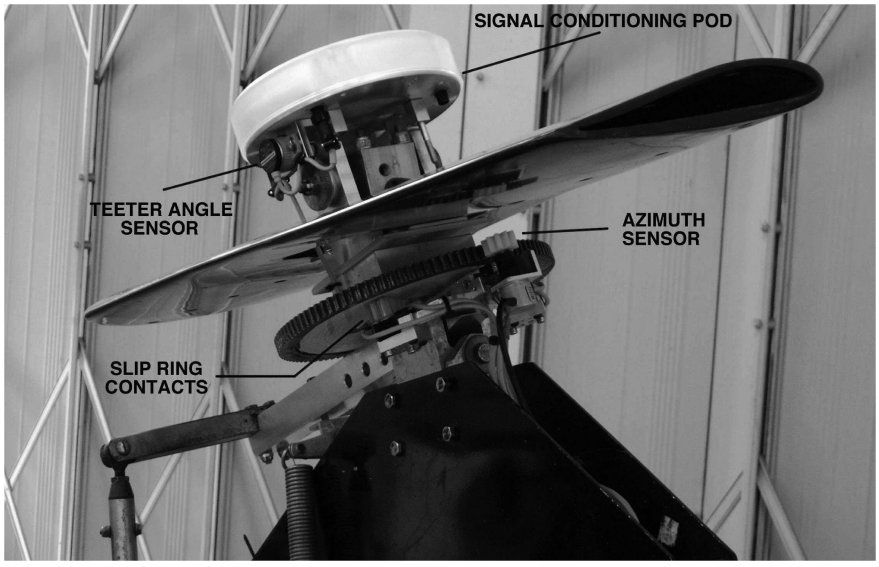

Fig. 2 Rotor head instrumentation.

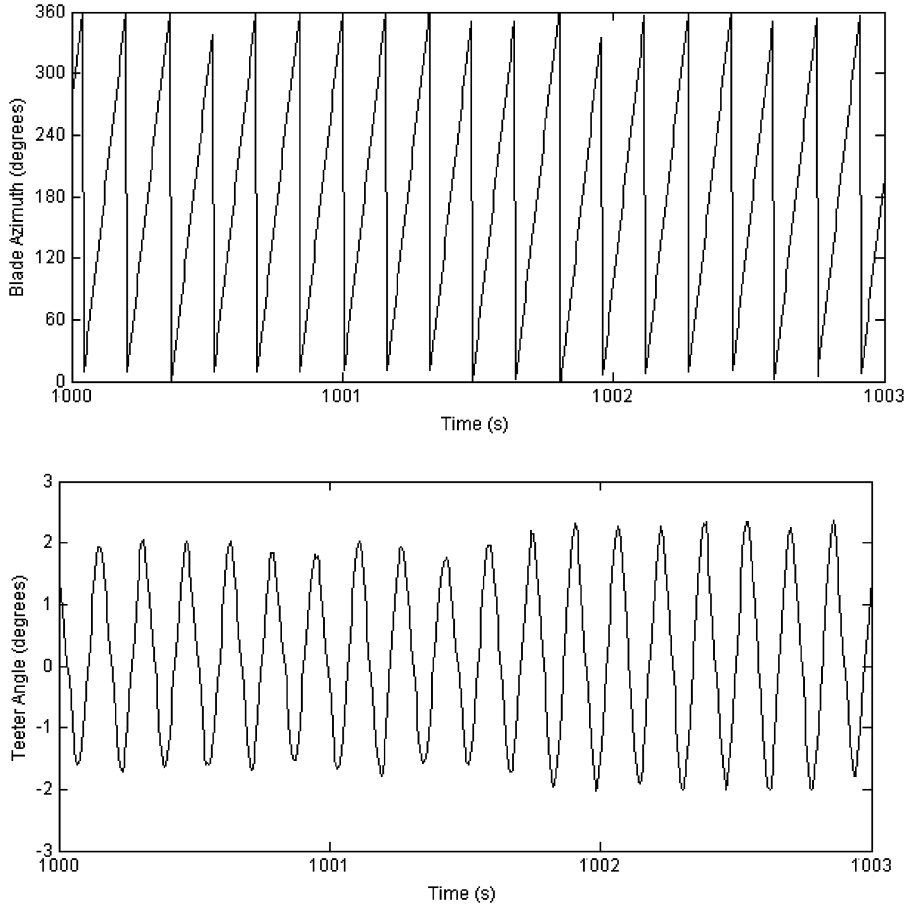

Fig. 3 Measured rotor azimuth and teeter angles.

$$\gamma = \frac{\rho a_1 c R^4}{I_\beta} \tag{18}$$

In principle, Eqs. (15–17) constitute three algebraic equations in the three unknowns v_0, v_{1s}, and v_{1c}. However, in this application, β_0 is not available because the two-bladed teetering rotor used cones by elastic deformation of the blades. An additional equation is therefore required, with coning becoming an unknown to be calculated. This equation is obtained from Eq. (2) by recognizing that $L_{\text{aero}} = M_{\text{aero}} = 0$; hence,

$$v_{1c} = (15/32)\pi \tan(\chi/2) v_0 \tag{19}$$

For the speed range studied, calculations show $\tan \chi/2 \approx 1$. However, if required, this can be refined using Eqs. (5) and (6) by assuming $v_{i0m} \ll w_{\text{hub}}$. Simulation modeling shows this is not unreasonable across the speed range examined.

Results

Figures 4–7 compare the flight-derived and corresponding engineering model values of the induced velocity and coning. Considerable scatter is present in some of these data; hence for clarity, linear trend lines are drawn through each set of points. The scatter is due to the variability in test conditions coupled with the unsteadiness of each test point that required averaging over a short period of time (typically 10 s) to obtain a trim value. The model is trimmed with actual flight-test data conditions; hence, the corresponding scatter in these results. The induced-velocity calculations, both flight and model, are presented in terms of body rather than wind axes. Data and calculation scatter provoke consideration of accuracy and error in these results. Note that fitting tools such as regression readily embrace consideration of error, and confidence bounds on the estimated parameter values can be calculated easily. However, in this application, the nature of the estimation, being an algebraic solution of three simultaneous equations in three unknowns, means that corresponding error bounds are nonpertinent. A more heuristic consideration of potential error sources is instructive, particularly because the statistical properties of any error are not known. Typical error sources are measurement and process; the former are minimized by careful calibration of sensors and the latter by use of an appropriate model structure that captures the essential behavior of the system. Use of what are trim equations for a dynamic process could give rise to process errors, but this is mitigated by choosing only slowly varying events in which the maximum change in, for example, airspeed is no more than ± 1 m/s. A sensitivity analysis of the effect of such a perturbation on the results is shown as error bounds on the calculated coning angle. The induced-velocity components vary by less than 1% (too small to show graphically) and, in effect, are insensitive to such variation in airspeed. The scatter in flight-derived variables then is indicative of the sensitivity of the results to random process errors. Coning, uniform, and longitudinal inflow coefficients display some variability in this respect, indicating robustness in the accuracy of these results. However, it is instructive to note the wide scatter in derived v_{1s}, consistent with an inappropriate model structure.

Figure 4 shows the uniform induced-velocity comparison. Generally, the flight and theory results agree to within 0.5 ms^{-1}, the discrepancy reducing with increased airspeed. This trend is consistent with interaction between propeller slipstream and main rotor for two reasons: 1) the configuration of the aircraft with its close-coupled rotor/propeller arrangement (Fig. 1) lends itself to such interaction; and 2) the variation of the propeller-induced velocity with airspeed, which simulation shows is approximately 10 ms^{-1} at low speed, decreases to 5 ms^{-1} at high speed. However, airframe interaction may also have a role to play. Elsewhere, significant discrepancy between wind-tunnel measurements and theoretical calculation of v_0

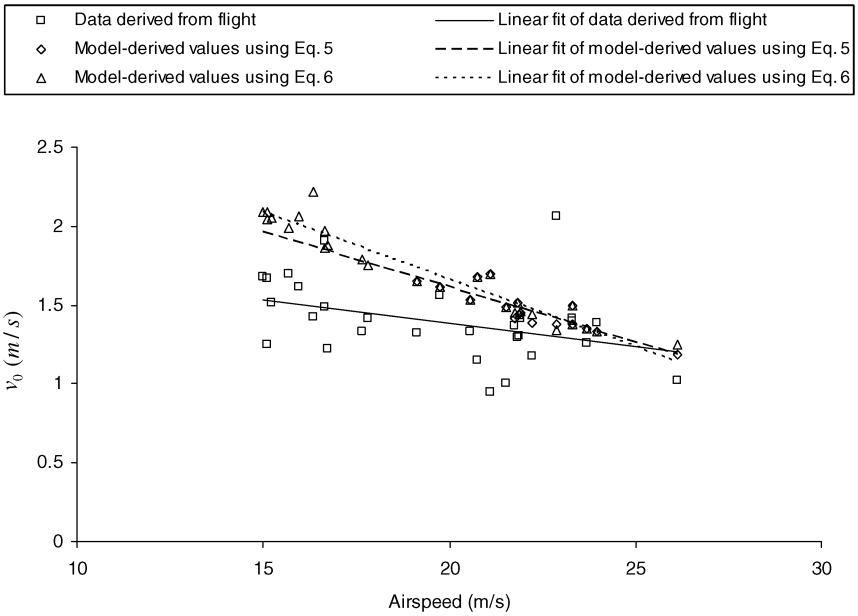

Fig. 4 Comparison of flight and model uniform induced-velocity components.

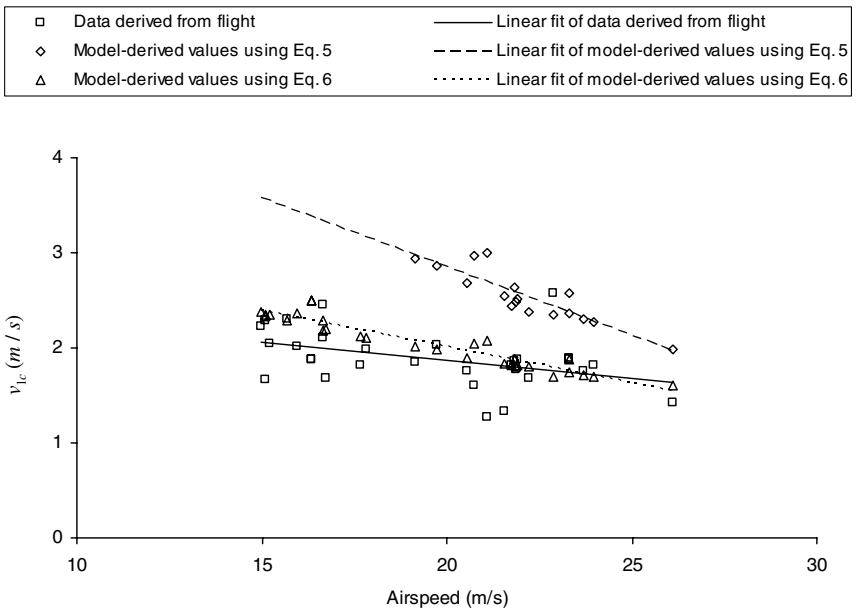

Fig. 5 Comparison of flight and model longitudinal induced-velocity components.

is attributed to equipment blockage effect [20], and the gyroplane fuselage may be acting in a similar manner that contributes to the result seen in Fig. 4. Figure 5 shows the longitudinal variation in the nonuniform component. Excellent agreement is obtained if the modulus of the mass flow term is retained in the skew angle expression shown in Eq. (6); whereas, a much poorer comparison is evident otherwise, although it does improve quickly with increased airspeed. The lateral component shows very considerable amounts of scatter and no correlation between flight and theory (Fig. 6). Theory indicates that, at best, there should be negligible (depending on the amount of sideslip) or zero lateral variation in the induced velocity. The values extracted from flight are, however, generally significant at about -1 ms^{-1}. Coning (Fig. 7) shows good correlation to within 0.5 deg across the speed range between values calculated from flight and theory. The most plausible explanation for the dissimilar trend with airspeed is elastic torsion of the blades. An audit of the relative magnitudes of the terms in Eq. (15) indicates that twist can contribute significantly to coning even for small values (of the order of only 0.25 deg/m). Therefore, unmodeled twisting, such as that from torsion, is likely to modify the coning of the rotor. Inclusion of elastic twist is a significant undertaking in models for rotorcraft flight mechanics and, as explained previously, rigid blade models are the norm. Accordingly in broad terms, the coning results are considered a verification of the approach to modeling teetering rotors [18].

The mismatch in the lateral induced-velocity component is worthy of further study. Figure 8 shows the lateral distribution of induced velocity when the flight mechanics model is coupled with a flowfield code designed specifically to model real-wake features [1]. Outboard of the 3 m station, there is symmetry between both sides of the disc, and these features are consistent with the rolled-up vortices trailed by the rotor that are familiar in appearance to the tip vortices trailed by an aeroplane wing. However, inboard of these stations, the distribution is asymmetric, and this is attributed to the influence of the propeller imposing an upwash component on one side of the main rotor and downwash on the other. If present in the flight-test data, the impact of these features on the longitudinal flapping will be mimicked by an

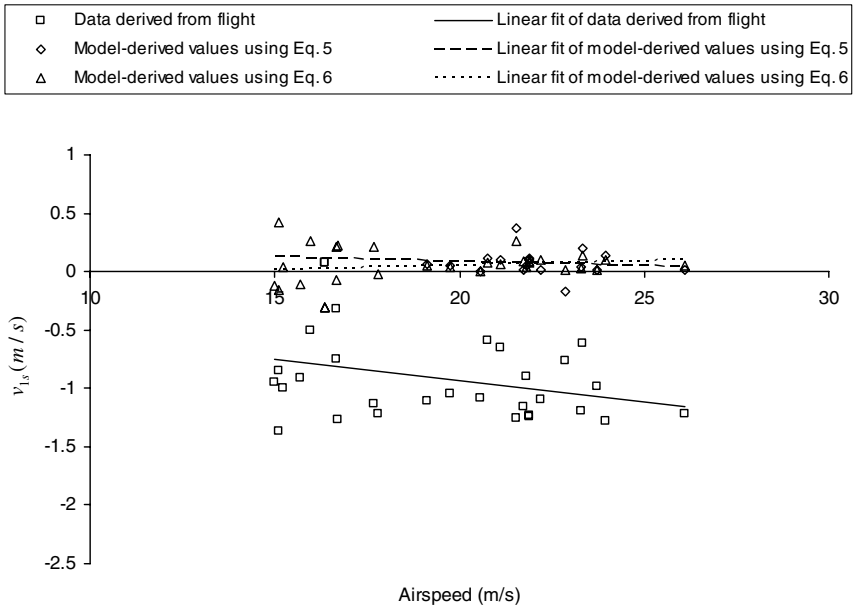

Fig. 6 Comparison of flight and model lateral induced-velocity components.

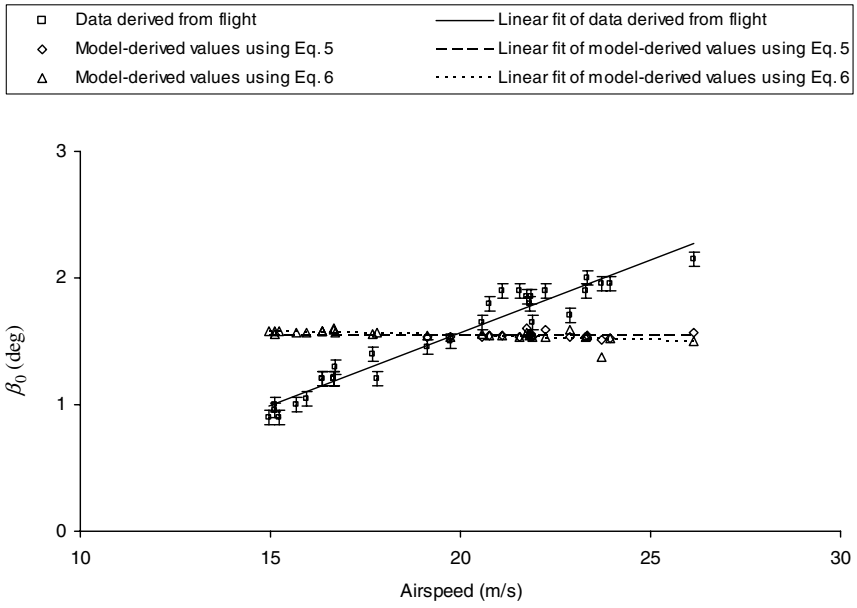

Fig. 7 Comparison of flight and model rotor-coning angles.

unrealistic value of v_{1s}, as it is impossible for the finite-state induced-velocity model to capture this distribution. This hypothesis is tested by comparing the longitudinal flapping angle calculated by the simulation model with three lateral induced-velocity distributions imposed: $v_{1s} = 0$ ms^{-1} (as calculated by the dynamic-inflow model); $v_{1s} = -1$ ms^{-1} (as derived from the flight-test data); and the distribution shown in Fig. 8. Figure 9 shows that the latter two distributions produce almost identical longitudinal flapping angles across the speed range, suggesting that $v_{1s} = -1$ ms^{-1} serves to mimic the full wake calculation.

Discussion

The simple model structure is effective in capturing the intimate relationship between flapping and inflow. Extraction of consistent and physically appropriate values of induced velocity, in the context of the approximation required to maintain a simple linear algebraic relationship, is testimony to the robustness of this relationship. This simplicity extends to the verification that is algebraic in nature due to the test points being trimmed flight. A more general verification of the intrinsic time-dependent nature of the model, using sophisticated parameter estimation numerical methods, relies on time-varying data from motions excited using specialized test inputs. It is recognized that this loss of generality is a limitation of the analysis here, but the results are still of relevance given the absence in the literature of verification in autorotation.

The objective was to validate the induced-velocity model for light gyroplane applications. Given the relatively low mass of this class of aircraft, it may be thought that the results lack more general applicability. However, comparison with a typical medium helicopter is instructive. For example, the gyroplane was operated at $C_T/\sigma =$ 0.076, and the Puma helicopter normally operates at $C_T/\sigma = 0.062$ in autorotation. The gyroplane tip-speed ratio is between 0.09 and 0.21; the Puma best-range autorotation airspeed is typical of most

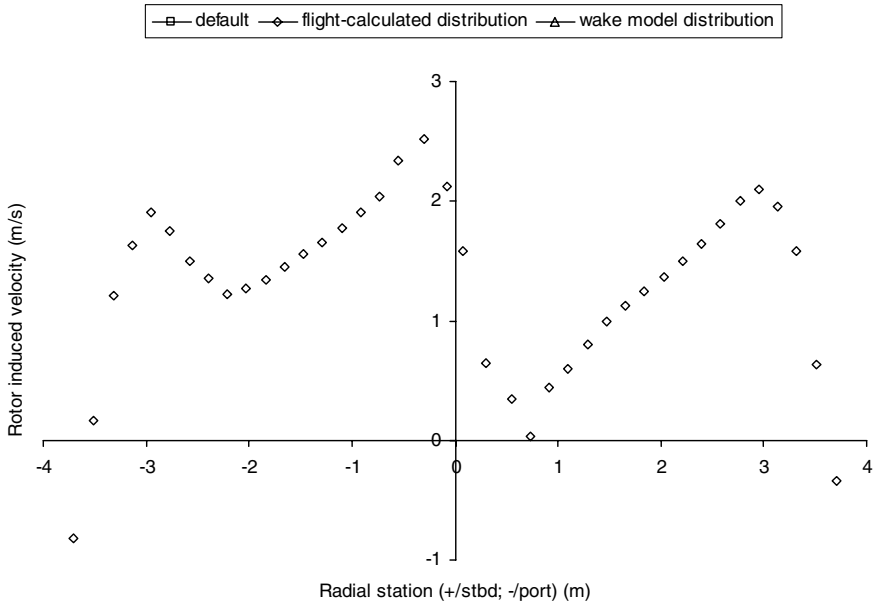

Fig. 8 Wake code, lateral induced-velocity distribution at 70 mph.

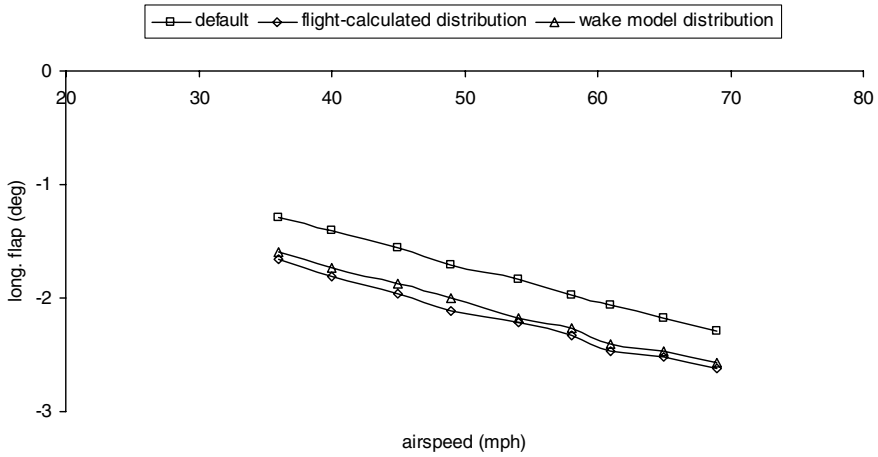

Fig. 9 Predicted longitudinal flap angle variation with three lateral induced-velocity distributions.

helicopters and is about 0.15. These verification results therefore, may be of wider applicability to autorotating rotorcraft in general.

The close-coupled pusher propeller design is known to demonstrate interactional aerodynamic phenomena. For example, in light gyroplane flying training, one effect of control that is demonstrated is the impact of propeller slipstream on main rotor speed. Such unmodeled interaction specific to the gyroplane layout appears to influence the induced-velocity results presented here in two ways. The first and most significant influence shows in the lateral component, in which correlation with flight is poor. The wake model results, however, do tend to suggest that the lateral induced-velocity distribution is dominated by the rolled-up trailed tip vortices and interaction with the propeller slipstream. The second and much less pronounced influence is in the uniform component at low speed, in which the propeller slipstream velocity is at its greatest. It is surmised then that the gyroplane's layout primarily renders the results configuration-specific in terms of the lateral induced-velocity distribution, with a secondary and much smaller effect on the uniform induced-velocity component at low flight speed.

Finally, the results tend to suggest that the wake skew angle should be represented with the modulus of the mass flow, consistent with the original Peters and Haquang formulation [2] in terms of disc angle of attack. Chen's review paper [16] presents skew angle without the modulus sign on the mass flow term and without comment. Geometrically, it is more appealing in that autorotations in which the wake cylinder skews above the rotor disc are modeled with angles greater than 90 deg. However, in terms of model fidelity, these results suggest that this appears to offer less accuracy.

Conclusions

Finite-state induced-velocity components can be extracted from rotor blade flapping data measured in flight. The Peters and Haquang dynamic-inflow model [2] generally offers good fidelity in replicating the uniform and longitudinal components of induced velocity across the rotor disc at typical rotorcraft thrust coefficients and airspeeds in autorotation. However, the model fails to capture the lateral variation that appears to be distorted significantly by unmodeled interactional aerodynamic phenomena unique to the pusher propeller aircraft configuration. These phenomena may also be responsible for a small discrepancy in the uniform component of inflow at very low airspeed. It is therefore concluded that further efforts may be needed to reach generalized validation of dynamic-inflow models for autorotation.

References

[1] Brown, R. E., "Rotor Wake Modeling for Flight Dynamic Simulation of Helicopters," *AIAA Journal*, Vol. 38, No. 1, Jan. 2000, pp. 57–63.
doi:10.2514/2.922

[2] Peters, D. A., and HaQuang, N., "Dynamic Inflow for Practical Applications," *Journal of the American Helicopter Society*, Vol. 33, No. 4, Oct. 1988, pp. 64–68.
doi:10.4050/JAHS.33.64

[3] Leishman, J. G., "Equation of Motion for Flapping Blade," *Principles of Helicopter Aerodynamics*, Cambridge Univ. Press, New York, 2000, pp. 134–138.

[4] Feik, R. A., and Perrin, R. H., "Identification of an Adequate Model for Collective Response Dynamics of a Sea King Helicopter," *Vertica*, Vol. 13, No. 3, 1989, pp. 251–266.

[5] Houston, S. S., "Identification of a Coupled Body/Coning/Inflow Model of Puma Vertical Response in the Hover," *Vertica*, Vol. 13, No. 3, 1989, pp. 229–250.

[6] Johnson, W., "Comparison of Calculated and Measured Helicopter Rotor Lateral Flapping Angles," *Journal of the American Helicopter Society*, Vol. 26, No. 2, Apr. 1981, pp. 46–50.

[7] Anon., "Airworthiness Review of Air Command Gyroplanes," Air Accidents Investigation Branch, Aldershot, England, U.K., Sept. 1991.

[8] Houston, S. S., "Identification of Autogyro Longitudinal Stability and Control Characteristics," *Journal of Guidance, Control, and Dynamics*, Vol. 21, No. 3, May–June 1998, pp. 391–399.
doi:10.2514/2.4271

[9] Houston, S. S., "Identification of Gyroplane Lateral/Directional Stability and Control Characteristics from Flight Tests," *Proceedings of the Institution of Mechanical Engineers, Part G: Journal of Aerospace Engineering*, Vol. 212, No. 4, 1998, pp. 271–285.

[10] Houston, S. S., "Validation of a Rotorcraft Mathematical Model for Autogyro Simulation," *Journal of Aircraft*, Vol. 37, No. 3, May–June 2000, pp. 403–409.
doi:10.2514/2.2640

[11] Thomson, D. G., Houston, S. S., and Spathopoulos, V. M., "Experiments in Autogyro Airworthiness for Improved Handling Qualities," *Journal of the American Helicopter Society*, Vol. 50, No. 4, Oct. 2005, pp. 295–301.
doi:10.4050/1.3092866

[12] Brown, R. E., and Houston, S. S., "Comparison of Induced Velocity Models for Helicopter Flight Mechanics," *Journal of Aircraft*, Vol. 37, No. 4, July–Aug. 2000, pp. 623–629.
doi:10.2514/2.2644

[13] Houston, S. S., "Validation of a Blade-Element Helicopter Model for Large-Amplitude Manoeuvres," *Aeronautical Journal*, Vol. 101, No. 1001, Jan. 1997, pp. 1–7.

[14] Peters, D. A., and He, C. J., "Correlation of Measured Induced Velocities with a Finite-State Wake Model," *Journal of the American Helicopter Society*, Vol. 36, No. 3, July 1991, pp. 59–70.
doi:10.4050/JAHS.36.59

[15] Murakami, Y., and Houston, S. S., "Dynamic Inflow Modeling for Autorotating Rotors," *Aeronautical Journal*," Vol. 112, No. 1127, Jan. 2008, pp. 47–53.

[16] Chen, R. T. N., "A Survey of Nonuniform Inflow Models for Rotorcraft Flight Dynamics and Control Applications," *Vertica*, Vol. 14, No. 2, 1990, pp. 147–184.

[17] Padfield, G. D., "Building a Simulation Model," *Helicopter Flight Dynamics*, 1st ed., Blackwell Science, Boston, 1996, pp. 93–94.

[18] Johnson, W., "Forward Flight II," *Helicopter Theory*, Dover, New York, 1980, pp. 235–238.

[19] Trchalik, J., Gillies, E. A., and Thomson, D. G., "Development of an Aeroelastic Stability Boundary for a Rotor in Autorotation," *AHS Specialist's Conference on Aeromechanics*, San Francisco, 23–25 Jan. 2008.

[20] Ellenrieder, T. J., and Brinson, P. R., "The Dynamic Induced Velocity Field of a Model Rotor in Hover Conditions," *Aeronautical Journal*, Vol. 102, No. 1016, June–July 1998, pp. 331–335.